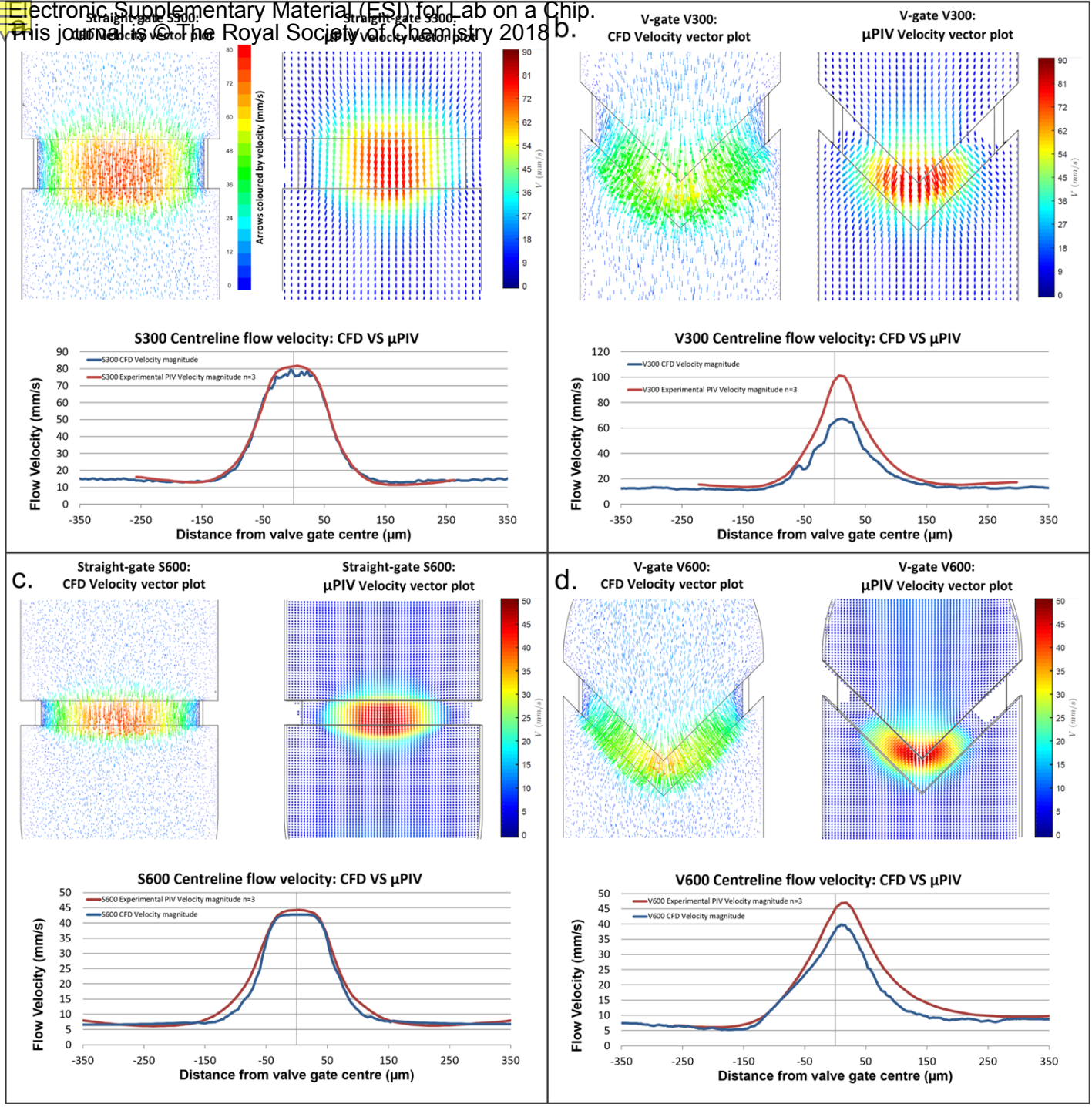

Supp fig 1 a. Direct comparison between velocity fields derived through computational fluid dynamic simulations (CFD), and corresponding experimental micro particle image velocimetry (µPIV) results, shown for 300µm straight **(a)** and v-shaped **(b)** valve gates and 600µm straight **(c)** and v-shaped **(d)**. This data is shown as velocity vectors with arrows scaled in size and coloured by magnitude, as well as centreline velocity plots superimposing longitudinal velocity along the centreline of the channel for both CFD and µPIV data. All data presented is representative of valves open to a height of 40µm at the centre of the valve gate, at Q=24 µl/min, with data shown for a central plane taken at 20µm, halfway between the valve gate and channel floor. All CFD results shown in this figure are simulated for water, in order to match µPIV conditions. CFD data is shown to match well to experimental results, with slight discrepancies most likely due to variances in individual valve actuation heights, potentially due to differing levels of delamination at the valve gate at low actuation pressures. Note the significant lateral component to fluid passing under V-shaped gates in b and d, as opposed to the relatively straight flow in a and c.

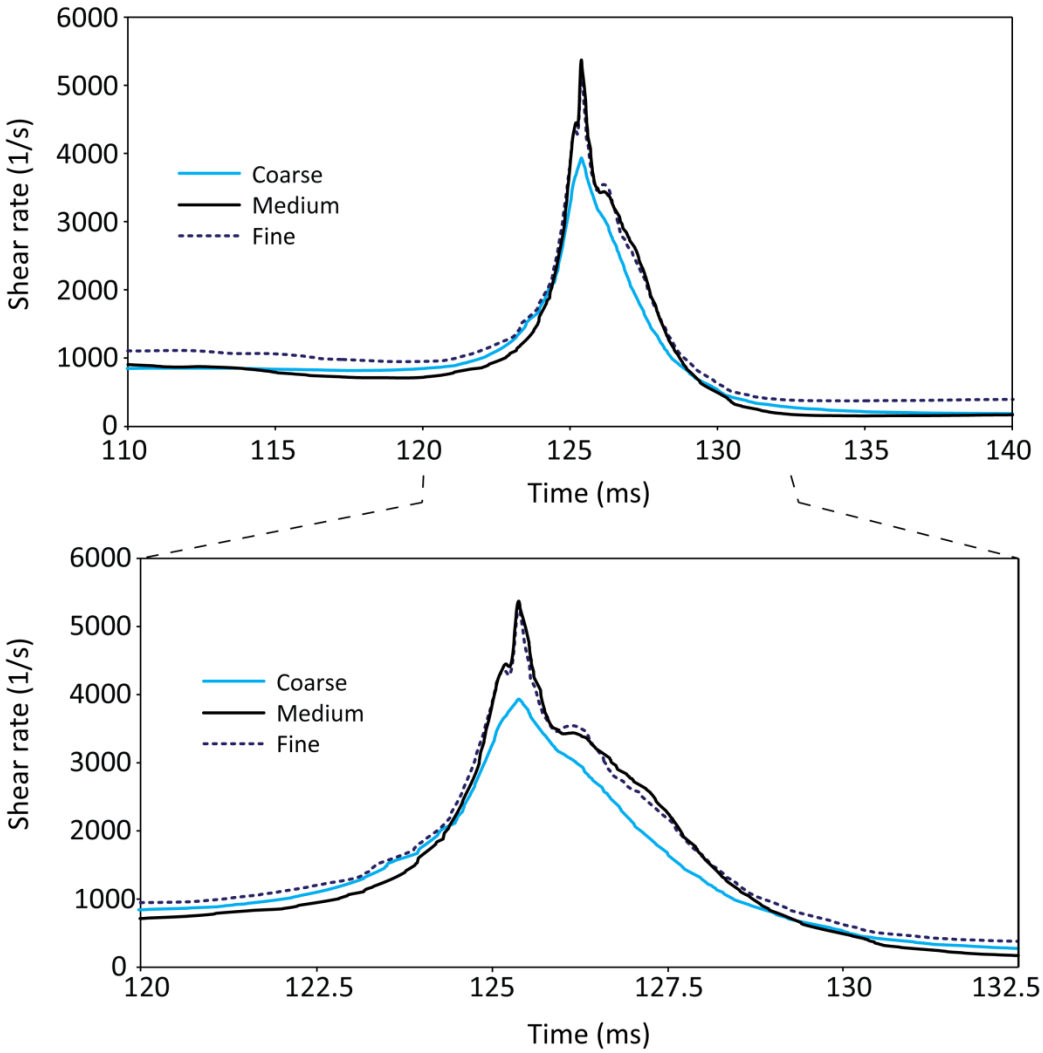

Supp fig 2. Grid convergence analysis of V-shaped gate, shear rate *v* time for a particle released 3 µm from the upstream of the V-300 gate and travelling along the middle of the gate. Simulations were conducted using three mesh densities, which are referred to as 'coarse', 'medium' and 'fine'. These mesh densities correspond to 90×15, 150×25, and 200×35 elements across the gate, respectively. A maximum shear rate of 3960 1/s was obtained using the ‘coarse’ mesh. Using the 'medium' mesh, the maximum shear rate increased to 5294 1/s. Applying the 'fine' mesh, the maximum shear rate only reduced to 5278 1/s with similar profiles observed before and after the gate, indicating grid convergence. Similar trends were obtained for the S300, S600 and V600 gates.

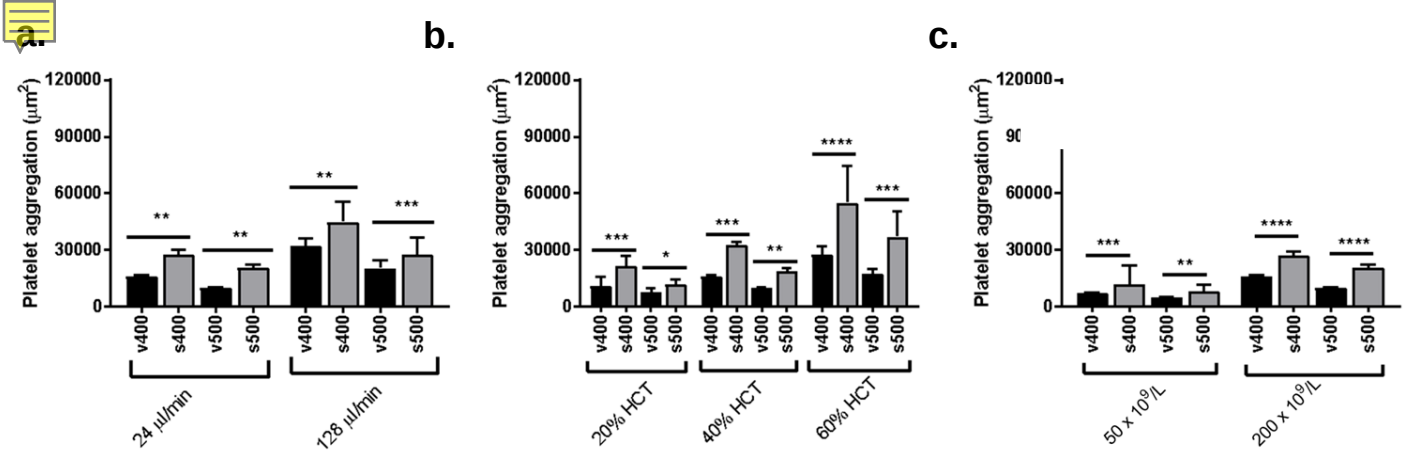

Supp fig 3 a. Platelet aggregation at straight versus v-gates at Q = 24 µl/min and 128 µl/min. **b.** Platelet aggregation at straight versus v-gates (Q = 24 µl/min) as a function of hematocrit. **c.** Platelet aggregation at straight versus v-gates (Q = 24 µl/min) as a function of platelet count. All data shows n=3 independent experiments normalized to valve surface area (µm^2). Error bars standard deviation. Black horizontal bars indicate comparative valve shapes and sizes (e.g. V300 and S300) for which a significance significant difference was tested for using a paired t-tests. * P ≤ 0.05, ** P ≤ 0.01, *** P ≤ 0.001, **** P ≤ 0.0001. * P ≤ 0.05, ** P ≤ 0.01, *** P ≤ 0.001, **** P ≤ 0.0001.

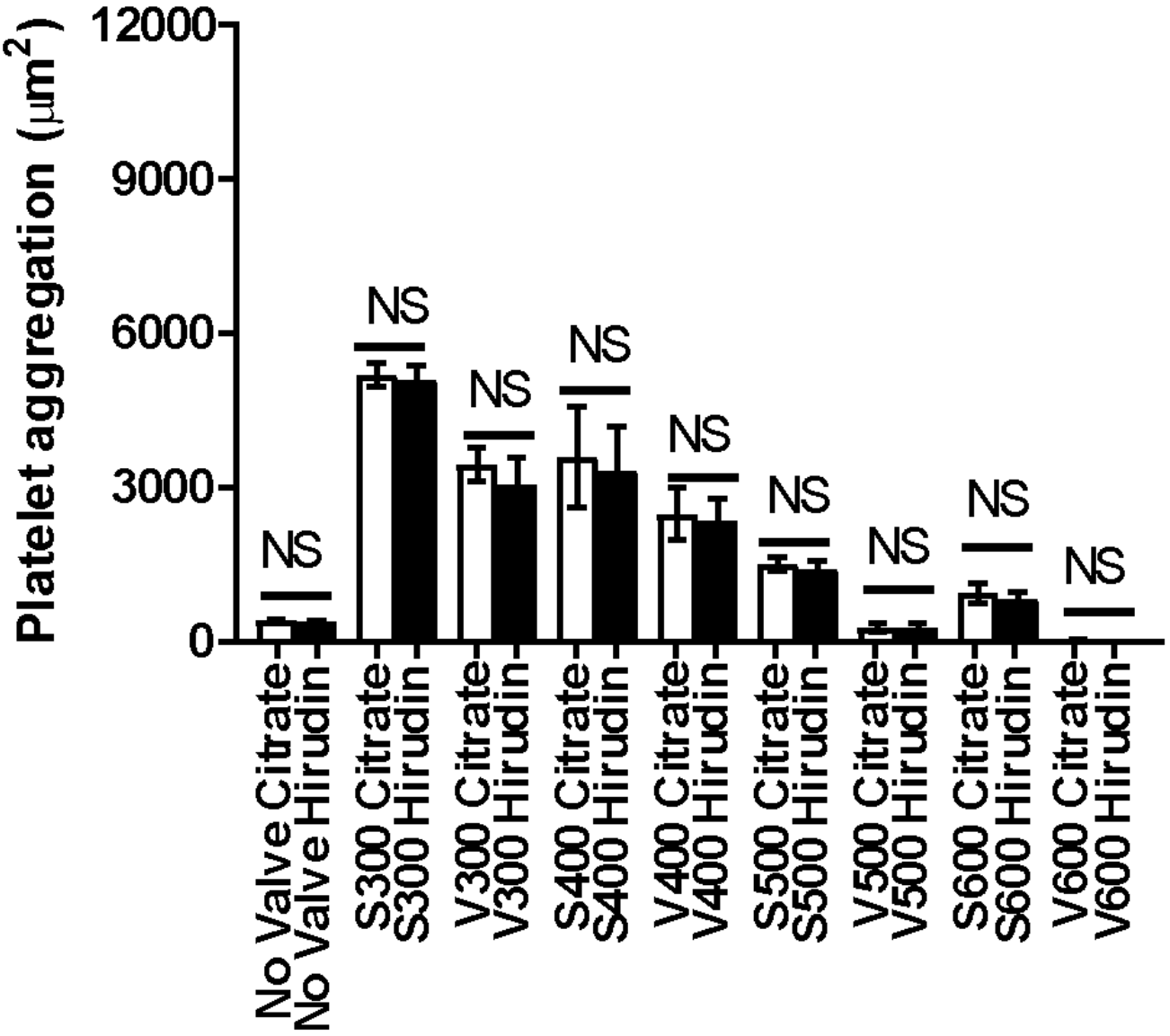

Supp fig 4 Comparison of aggregate sizes with blood collection into Hirudin (0.02% w/v) and Citrate (2% w/v) anticoagulants. Platelet aggregation was measured at Q = 24 µl/min and all valves were fully actuated. Data shows n=3 independent experiments normalized to valve surface area (µm^2). Error bars indicate standard deviation. Black horizontal bars indicate comparative valve shapes and sizes (e.g. V300 and S300) for which a significance significant difference was tested for using a paired t-tests. NS = no statistically significant difference, * $P \leq 0.05$, ** $P \leq 0.01$, *** $P \leq 0.001$, **** $P \leq 0.0001$.

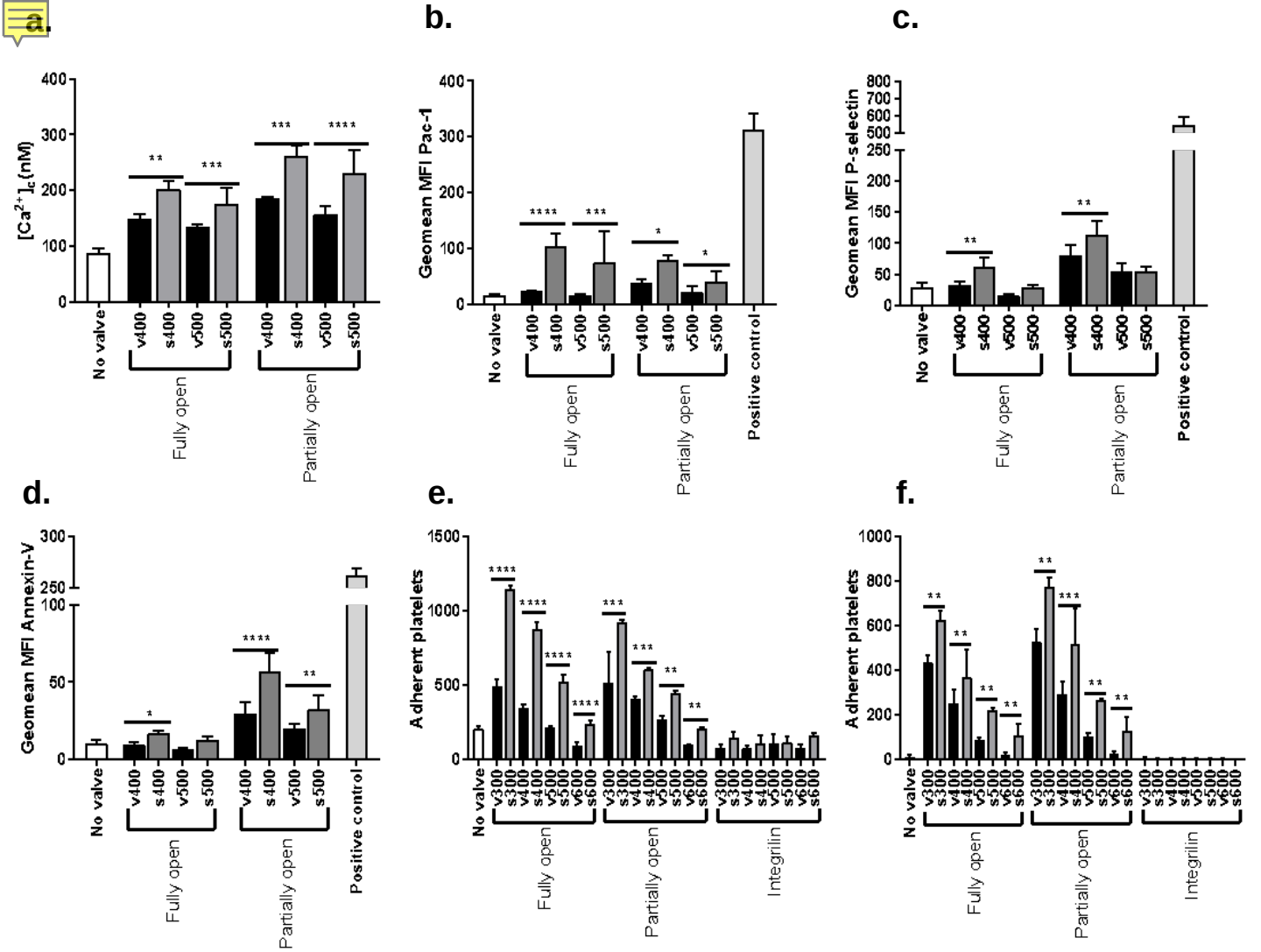

Supp fig 5 a. Maximal platelet cytosolic calcium flux $[Ca^{2+}]_c$ (nM) under perfusion at Q = 24 µl/min in the fully open and partially open (40 µm) states. (n=3 independent experiments). **b**. Fluorescence Activated Cell Sorting (FACS) analysis showing Mean Fluorescence Intensity (MFI) GeoMean distribution of FIT-C PAC-1 antibody binding (integrin $\alpha_{IIb}\beta_3$ activation) to platelets in human whole blood following perfusion through S400, S500, V400 and V500 gates (Q = 24 µl/min) in the fully open and partially open (40 µm) states. **c**. FACS analysis showing MFI GeoMean distribution of expression of P-selectin antibody binding to platelets in human whole blood following perfusion through S400, S500, V400 and V500 gates (Q = 24 µl/min) in the fully open and partially open (40 µm) states. **d**. FACS analysis showing MFI GeoMean distribution of FITC- Annexin-V binding to platelets in human whole blood following perfusion through S400, S500, V400 and V500 gates (Q = 24 µl/min) in the fully open and partially open (40 µm) states. **e.** Total number of adherent (captured) platelets in a vWF-coated (10 µg/ml) microchannel 1,000 µm post valve passage at t=130 seconds following perfusion at a straight channel shear rate of 1,800.s^{-1}. **f.** Total number of adherent (captured) platelets in a fibrinogen-coated (13 µg/ml) microchannel 1,000 µm post valve passage at t=130 seconds following perfusion at a straight channel shear rate of 300.s^{-1}. All data indicates n=3 independent experiments normalized to valve surface area. Error bars indicate standard deviation. Black horizontal bars indicate comparative valve shapes and sizes (e.g. V300 and S300) for which a significance significant difference was tested for using a paired t-tests. * P ≤ 0.05, ** P ≤ 0.01, *** P ≤ 0.001, **** P ≤ 0.0001. * P ≤ 0.05, ** P ≤ 0.01, *** P ≤ 0.001, **** P ≤ 0.0001.

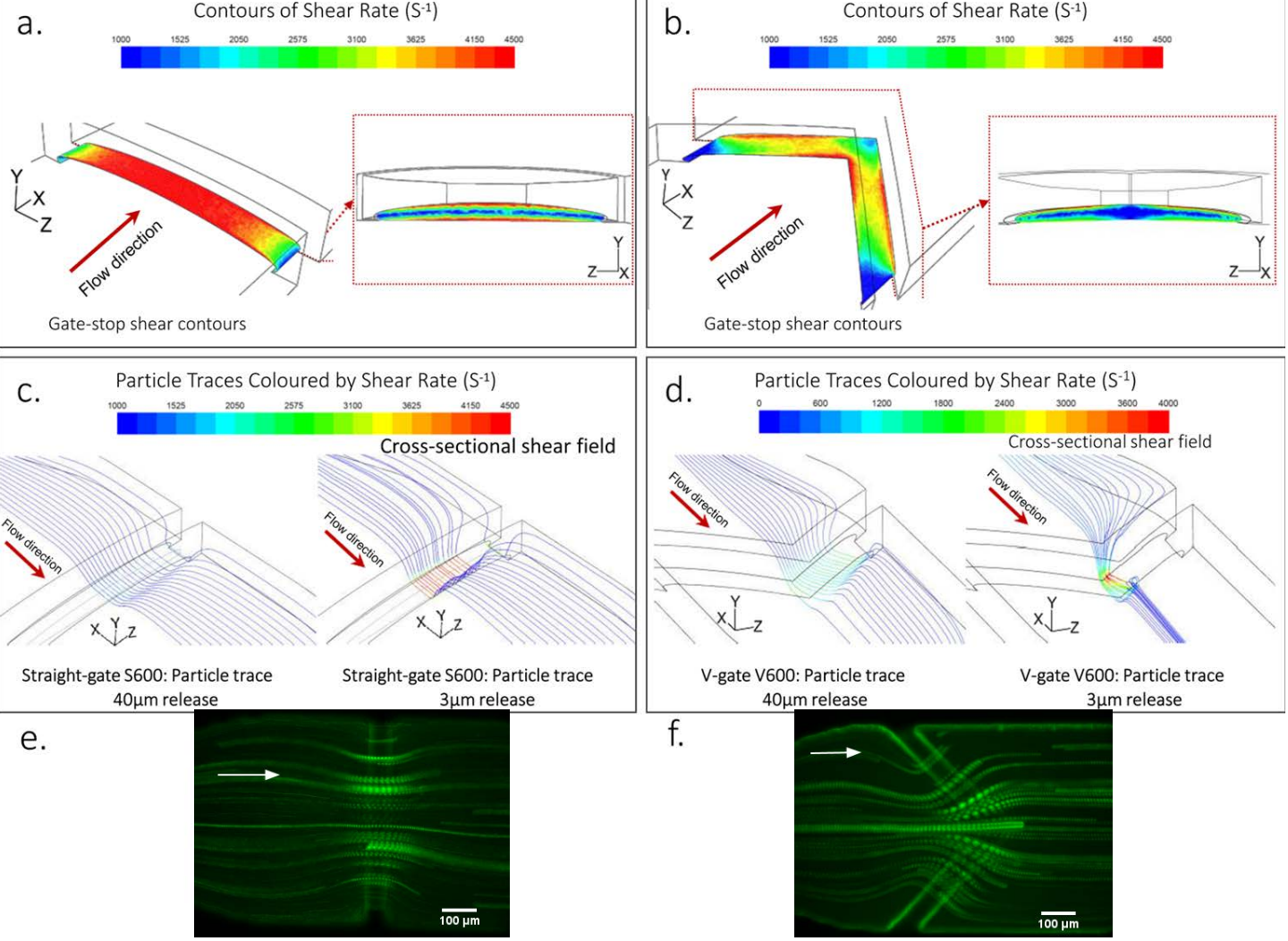

Supp fig 6. a. 3-dimensional shear contour profiles of S600 gate geometry at Q=24 ml/min and opening height of 40mm. Note the peaks in shear rate at the upstream and downstream edges of the straight gate and the overall elevation in shear rate across the straight gate surface. b. 3-dimensional shear contour profiles of V600 gate geometry at Q=24 ml/min and opening height of 40mm. Note the initial peak in shear rate at the midline upstream face of the gate surface and overall reduced shear rates. Note the generation of a low shear rate pocket that extends across the microchannel cross-section. c. Particle shear rate streamlines for fifteen 2mm particles released 40mm and 3mm from the microchannel ceiling for the straight gate case. Note the parallel particle trajectories across the gate surface. d. Particle shear rate streamlines for fifteen 2mm particles released 40mm and 3mm from the microchannel ceiling for the v-gate case. Note the streamline “funneling” for particles released at 3mm towards the valve gate midline. Note the loss of funneling at 40mm from the microchannel ceiling and divergent particle trajectories across the v-gate surface. e. Superimposed imaged of particle streamline flows taken from 16 seconds of flow in partially open S600 valves f. Superimposed imaged of particle streamline flows taken from 16 seconds of flow in partially open V600 valves.

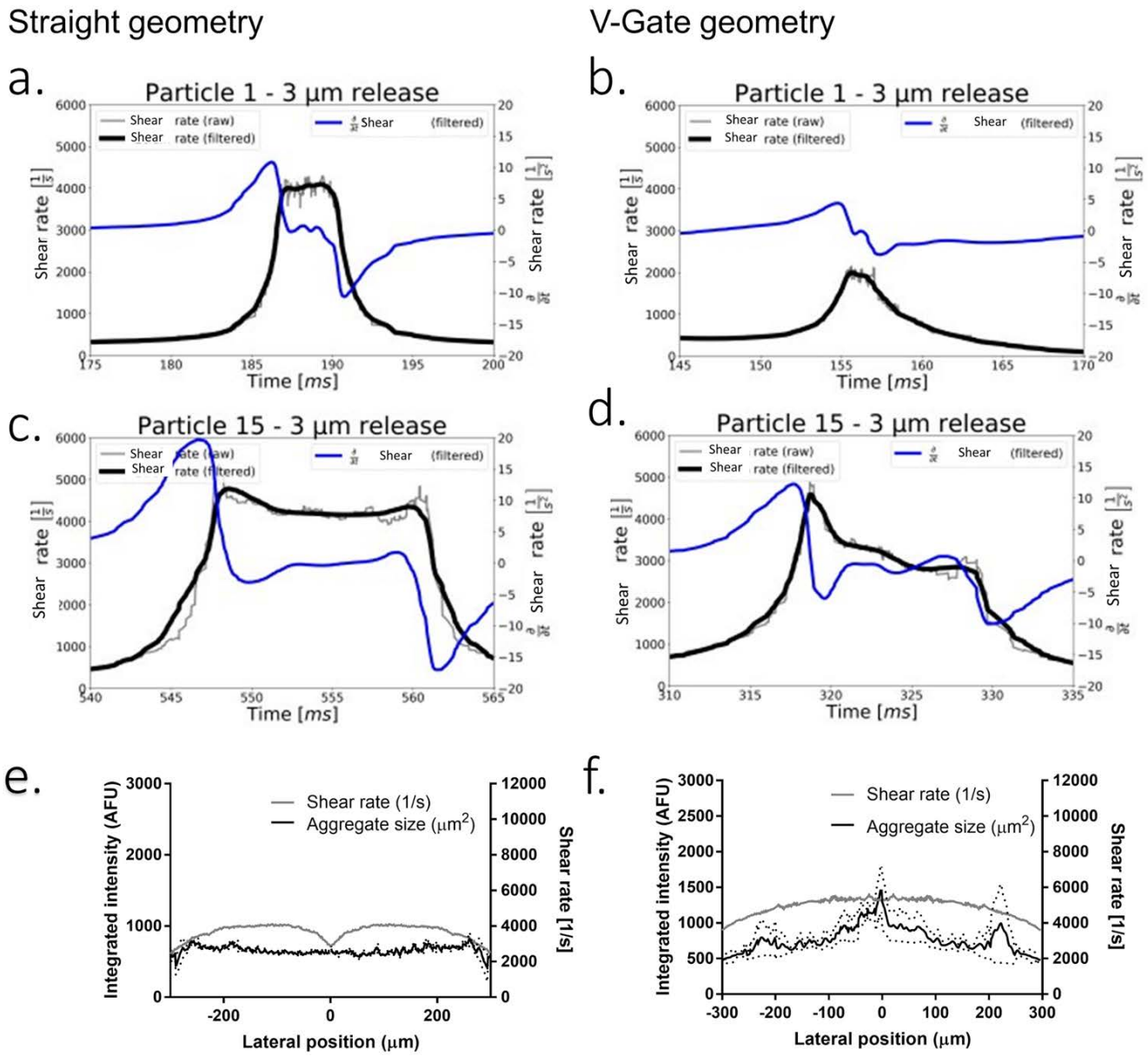

Supp fig 7 a-d. Particle shear rate (s^{-1}) v time (black line) and shear rate gradient (s^{-1}/s) (blue line) plots for particles released 3µm from the microchannel ceiling. Particle 1, released at the channel midlines is shown in the straight geometry (a) and v-gate (b), while particle 15, released at the lateral margin, close to the channel sidewall, is shown for the straight geometry in (c) and the v-gate in (d). Note the symmetric shear rate and shear rate gradient profiles for the straight case versus the asymmetric distribution and the overall reduction in peak shear rate for the v-gate. Particle 15 in both cases displayed extended shear profiles due to sidewall effects and the overall upward deformation of the valves in the open state. e-f. Points of maximal platelet aggregation and shear across the V600 partially open (40 µm) (e) and S600 partially open (f) as a function of distance from the valve midpoint. All data shows n=3 independent experiments. Error bars indicate standard deviation.

Valve Dimensions: V-600 Example case

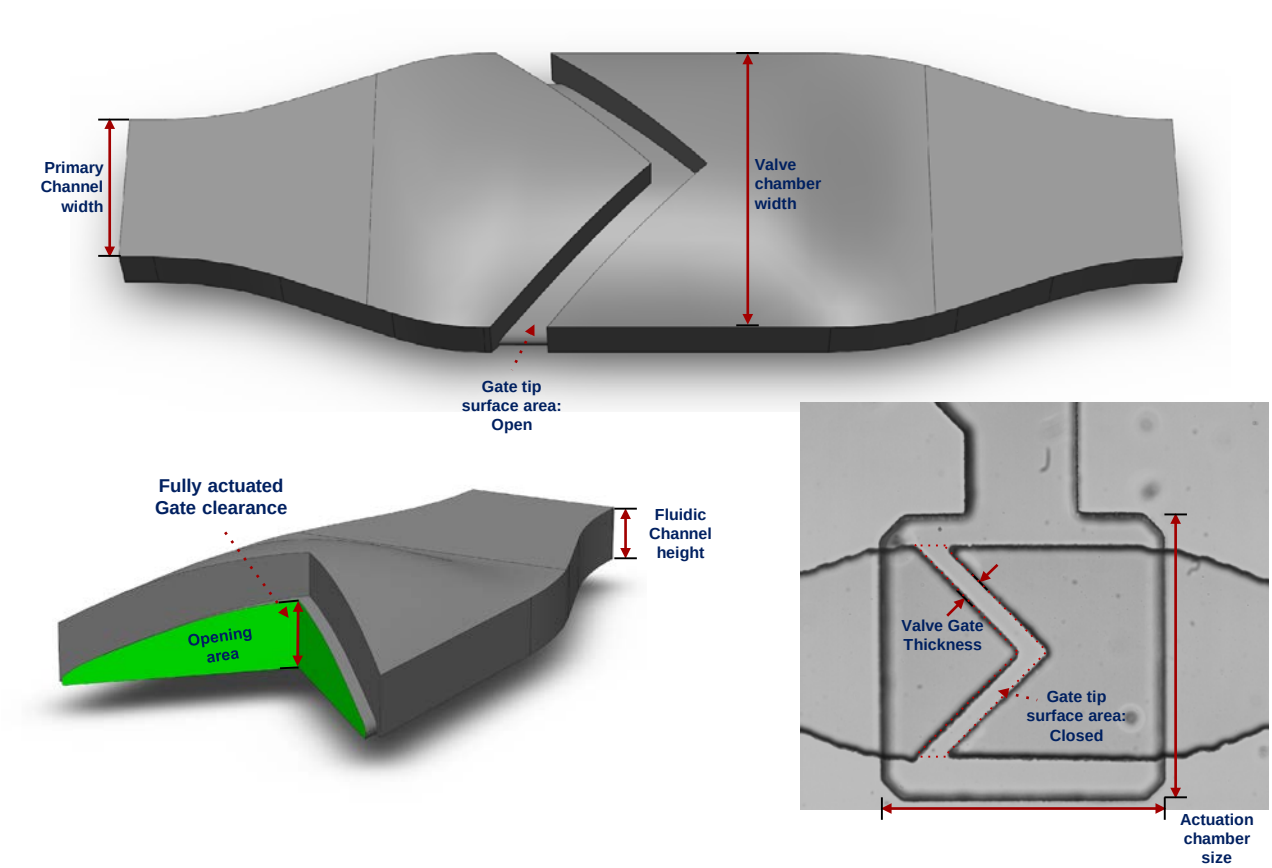

Valve name	Valve gate geometry	Fluidic Channel height	Primary Channel width	Valve chamber width	Actuation chamber size	Actuation chamber Depth	Actuation membrane thickness	Valve Gate Thickness	Fully actuated Gate clearance	Opening area	Gate tip surface area: Closed	Gate tip surface area: Open
S 300	Straight	100 µm	300 µm	300 µm	500 X 500 µm	150 µm	30-50 µm	50 µm	44 µm	0.01184 mm^2	0.0135 mm^2	0.01599 mm^2
S 400	Straight	100 µm	300 µm	400 µm	600 X 600 µm	150 µm	30-50 µm	75 µm	73 µm	0.01932 mm^2	0.02877 mm^2	0.03207 mm^2
S 500	Straight	100 µm	300 µm	500 µm	700 X 700 µm	150 µm	30-50 µm	75 µm	107 µm	0.0363 mm^2	0.03609 mm^2	0.04228 mm^2
S 600	Straight	100 µm	300 µm	600 µm	800 X 800 µm	150 µm	30-50 µm	75 µm	124 µm	0.05171 mm^2	0.04288 mm^2	0.05006 mm^2
V 300	V - Gate	100 µm	300 µm	300 µm	500 X 500 µm	150 µm	30-50 µm	50 µm	52 µm	0.01398 mm^2	0.01856 mm^2	0.02183 mm^2
V 400	V - Gate	100 µm	300 µm	400 µm	600 X 600 µm	150 µm	30-50 µm	75 µm	86 µm	0.02496 mm^2	0.0485 mm^2	0.05539 mm^2
V 500	V - Gate	100 µm	300 µm	500 µm	700 X 700 µm	150 µm	30-50 µm	75 µm	118 µm	0.04072 mm^2	0.04871 mm^2	0.05508 mm^2
V 600	V - Gate	100 µm	300 µm	600 µm	800 X 800 µm	150 µm	30-50 µm	75 µm	133 µm	0.0642 mm^2	0.06013 mm^2	0.06775 mm^2

Supp table 1 Valve dimensions

Dimensions of valve geometries used in this study. Valve name is the name each valve type is referred to throughout the manuscript, valve gate geometry classifies the two types of valve investigated. Fluidic channel height is the height of the fluidic channels, while primary width is the width of the primary channel leading to the individual gates. Valve chamber width refers to the width of the expanded channel area at the valve gate, or length of the valve, while actuation chamber size defines the size of the pneumatic actuation chamber situated above each valve, and actuation chamber depth is the depth of this chamber. Actuation membrane thickness is the thickness of the PDMS membrane separating the valve channel roof and actuation chamber, gate thickness is the thickness of the gate itself. Fully actuated gate clearance refers to the opening height at the centre of the valve gate under minimum pressure, or fully open conditions, while opening area is the cross sectional area of the gate when fully open. Gate tip surface area when closed refers to the area of the valve gate in contact with the channel floor in the closed configuration, while gate tip surface area open refers to the area of the valve gate tip when fully expanded in the open configuration

Coefficients[a]

Model		Unstandardized Coefficients		Standardized Coefficients	t	Sig.
		B	Std. Error	Beta		
1	(Constant)	-22596.135	3484.757		-6.484	.000
	V_shaped_valve	28136.695	2530.866	.750	11.117	.000
	Straight_valve	39075.299	2530.866	1.041	15.439	.000
	Valve_size	-8202.348	542.401	-.563	-15.122	.000
	HCT	449.107	60.642	.229	7.406	.000
	Plt_count	11903.215	1855.466	.202	6.415	.000
	Flow_rate	13763.773	1855.466	.234	7.418	.000
	Open_state	31936.131	1961.298	.515	16.283	.000

a. Dependent Variable: Aggregate_size

Supp table 2 Multifactorial analysis

A multiple regression was run to predict aggregate size from valve geometry, size, patient Hct, platelet count, flow rate and open state. These variables statistically significantly predicted aggregate size, $F(7, 236) = 116.218$, $p < 0.0005$, $R^2 = 0.780$. All six variables added statistically significantly to the prediction, $p < 0.0005$. The unstandardised coefficients demonstrate effect size.

Supplementary Materials & Methods

Micro particle image velocimetry (μPIV)

Micro-PIV was used to Verify and Support CFD models. Velocity field was assessed at measurement planes located halfway between the bottom surface of the channel and the tip of the valve stop. An inverted TI-U Eclipse Nikon microscope equipped with an air-immersion CFI S Plan Fluor ELWD 20× objective lens was coupled with a high-speed camera (2277 Hz at 2000 × 2000 pixels, 12 bits, PCO.dimax HS4) to record the particle images. One micron diameter red fluorescent polystyrene aqueous beads (ThermoFisher Scientific) were used to seed the flow. Polysorbate 20 (Tween 20) was added to flow to avoid particle-wall adhesion to and to prevent particle agglomeration. Illumination was provided by a 532 nm Nd:YAG double-pulsed laser (EverGreen - BigSky Laser Series) able to double-pulse at 15 Hz. A syringe pump (Harvard PHD ULTRA) and a gas-tight glass syringe (1000 μL, Hamilton) were used to deliver fluid into the microchannel via a silicon tube.

Measurements were taken at flow rates of 24 μL/hr in all channels with V-type and Straight-type valves at two different valve positions (fully opened and 40 μm open). In each set of measurements, 4000 images were captured. The common background noise in micro-PIV recordings were removed by subtracting the background image (acquired by averaging 100 images) from each recording. In micro- PIV usually low seeding density is used to reduce the background noise due to the out-of-focus particles, thereby reducing the signal to-noise ratio in correlation maps. Two averaging method (“Average Image Method” and “Average Velocity Methods”) were employed to enhance the signal-to-noise. In the first method 20 images were overlaid to increase the number of particle per interrogation window (Average Image Method). Then a multigrid algorithm combined with window deformation algorithm with adaptive central difference interrogation (CDI) offsetting was implemented. Using a Fast Fourier Transform based cross-correlation algorithm, the local displacements correspond to each interrogation window (32×32) were acquired. The depth of correlation and the spatial resolution of the micro-PIV measurement were 7, 8 and 9 μm, respectively. The valid vectors of each realisation were identified using a median test and were then averaged over all realisation window (Average Velocity Method).

Assessment of platelet streamline flow

To image platelet streamlines across microvalve gate surfaces isolated platelet suspensions ($200x10^9$/L) in platelet washing buffer (4.3 mM K_2HPO_4, 4.3 mM Na_2HPO_4, 24.3 mM NaH_2PO_4, 113 mM NaCl, 5.5 mMD-glucose, and 10 mM theophylline, pH 6.5) + Integrillin (20mg/mL) were labelled with the lipophilic membrane dye DiOC6 (1μg/mL) (Molecular Probes) and 0.02U/mL apyrase (to eliminate released ADP during blood collection) for 10 min at 37^{o}C and subsequently perfused through the device at constant flow rate of 24 μL/min. Fluorescent platelet streamlines were acquired on an inverted Nikon TiU microscope (Nikon Plan Fluor 20x/0.50 objective) using an Andor Zyla sCMOS camera at 10msec exposure time, 15fps for 60sec. Time-lapse tiff imaging stacks were processed to remove background fluorescence and filtered using a median filter (2x2 kernel). Tiff stacks were subsequently processed via average z-projection to create average heat map distributions of platelet trajectories using a 16-color LUT.